ON NON-LOCAL EFFECTS OF ECE MEASUREMENTS AT W7-AS

N.B. Marushchenko, H. Maaßberg, H. Hartfuß, A. Dinklage

Max-Plank-Institut für Plasmaphysik, EURATOM-Association, Greifswald, Germany

e-mail: nikolai@ipp.mpg.de

The role of the intrinsic non-locality of the EC emission is described with respect to the ECE diagnostic at W7-AS. As a fairly extreme example, a low density ECRH discharge with high electron temperature and very strong gradients is analysed, and the lowest limit of spatial resolution of the ECE measurements is determined.

The basic assumptions of "standard" ECE electron temperature measurements are i) a highly localized emission in a sufficiently narrow frequency range (frequency band of the reciever), and ii) the equivalence of the spectral intensity (being measured) and the local electron temperature. Especially at higher T_e, the spatial region of the local emission is significantly broadened due to the relativistic down-shift in the frequency, and the measured emission is essentially narrowed for high reabsorption. Furthermore, in high power ECRH discharges at low densities, a population of suprathermal electrons appears in the deposition region, which can significantly affect the ECE spectrum making the interpretation more complex. But even with this additional suprathermal emission omitted, it is necessary to determine the spatial resolution of ECE measurements and the impact on the T_e profile evaluation.

The aim of this work, similar to [1], is to estimate the limitation of the spatial resolution in the ECE diagnostic coming from the intrinsic non-locality of the EC emission. This analysis is very important for the concept of the ECE evaluation in the new generation stellarator W7-X (under construction in Greifswald, Germany), and we must avoid these problems in the "standard" ECE evaluation where the spectral intensity,I_ω, measured in a narrow frequency channel, ω, is interpreted as the "local" electron temperature. As an example, where the non-local effects of the ECE are fairly strong, a W7-AS discharge with a highly peaked electron temperature profile is analysed.

The ECE measurements at W7-AS were performed by a radiometer at the 2nd harmonic X-mode which is positioned at the low-field-side. For optimum conditions, the ECE system is placed at the "elliptical" plane, i.e. the cross-section with a strong toroidal curvature leading to a sufficient gradient of the magnetic field strength along the horizontal chord allowing for a

fairly good localization of the emission. The variation of B is small enough to avoid harmonic overlapping ($\Delta B/B \simeq 24\%$ corresponding to $2\Delta f_c \simeq 34$ GHz across the plasma with $2f_c \simeq 140$ GHz on axis), i.e. the emission is related only to one (2nd) cyclotron harmonic. Usually the plasma is optically thick for the X2-mode, and for rather low electron temperatures ($T_e \lesssim 1$ keV), mainly the characteristics of radiometer (the width of frequency bands, δf, and the distance between them) are responsible for the spatial resolution δR of the ECE measurements. In the local ("cold") approach, the spatial resolution can be estimated as $\delta R_c \simeq \delta f/f \cdot B(\partial B/\partial R)^{-1}$, which for the bandwidth of $\delta f = 0.3$ GHz should give a perfect spatial resolution, $\delta R_c \simeq 2$ mm.

Two effects are responsible for the ECE line broadening measured outside of the plasma: i) the relativistic effect leading to a frequency down-shift, i.e. the main contribution of the "local" emission for a fixed frequency is coming from the region behind the "cold resonance" layer, from the high-field side, and ii) the reabsorption at lower B, i.e. close to the "cold resonance". Consequently, the measured spectral intensity, I_ω, is determined by the balance of both effects. This means, that a "local" interpretation of the measured I_ω spectra leads to a systematic inward-shift to higher B (with respect to the "cold resonance" position), and that the spatial resolution is always smaller than the local ("cold") one, i.e. $\delta R_r \delta R_c$. Even a very rough estimation of the spatial resolution for slightly relativistic electrons using only the relativistic resonance condition leads to a 1st order correction: $\delta R_r \simeq \delta R_c + T_e/mc^2 \cdot B(\partial B/\partial R)^{-1}$, and $\delta R_r \simeq 1$ cm is obtained for $T_e = 5$ keV compared to $\delta R_c \simeq 2$ mm in the "cold" (standard) approach.

The radiative transport equation [2] describing the balance of local emision and reabsorption can be written in the form

$$I_\omega(s) = I_\omega^{inc}(-a)\,\mathrm{e}^{-\tau_\omega(s)} + \int_{-a}^{s} \mathrm{d}s'\,\eta_\omega(s')\,\mathrm{e}^{-\left(\tau_\omega(s)-\tau_\omega(s')\right)} \qquad (1)$$

where $I_\omega(s)$ is the spectral intensity at the position s along the chord ($I_\omega = I_\omega(a)$ is measured outside of the plasma), $\tau_\omega(s)$ is the optical depth [3] defined as the absorption coefficient, $\alpha_\omega(s')$ (in relativistic approach), integrated along the chord up to s, and $\eta_\omega(s')$ is the emission coefficient. Only for a Maxwellian distribution function, η_ω and α_ω fulfill the relation: $\eta_\omega(s') = \omega^2/8\pi^3c^2 \cdot T_e(s')\,\alpha_\omega(s')$.

The first term in Eq.(1) desribes the contribution of radiation reflected from the inner high-field-side wall, $I_\omega^{inc}(-a)$. In order to supress this disturbing contribution, a special keramic absorber was installed at the inner wall in the sightline of the ECE antenna. Thus, the first term of Eq.(1) can be omitted. Assuming a very high optical depth close to the "cold resonance" layer and a fairly flat $T_e(s') \simeq T_e(s)$, Eq.(1) can be reduced to the

usual definition of the radiative temperature, T_{rad},

$$I_\omega \simeq \frac{\omega^2}{8\pi^3 c^2}\, T_{rad}(s_*) \left(1 - \mathrm{e}^{-\tau_\omega(a)}\right) \simeq \frac{\omega^2}{8\pi^3 c^2}\, T_{rad}(s_*) \qquad (2)$$

where the location of emission, s_*, is usually approximated by the "cold resonance" condition. The coefficient in Eq.(2) is defined following Kirchhoff's law, but in practice this constant contains a lot of other hidden factors and has to be determined by a black-body calibration of the complete ECE system. Exactly this Eq.(2) is the usual basis for the ECE diagnostics.

The local absorption coefficient scales roughly with $\alpha_\omega(s') \propto n_e(s')\, T_e(s')$, thus $\eta_\omega(s') \propto n_e(s')\, T_e^2(s')$ strongly increases with T_e. For stronger gradients $\partial T_e/\partial s'$, two effects are observed: i) the value of the radiative temperature, T_{rad}, is an average over the emission region weighted by the exponential in the integrand of Eq.(1) which describes the reabsorption, and ii) the location of emission, s_*, is additionally shifted, where this additional shift has different signs for the high-field-side and low-field-side. For the high-field-side, the electron temperature gradient reduces the non-locality ($\partial B/\partial s'$ and $\partial T_e/\partial s'$ have different signs) whereas for the low-field-side measurements the non-locality is increased. Then the "local" T_{rad} estimation for the high-field-side is more reliable compared to the low-field-side. This tendency strengthens also the asymmetric spatial resolutions from the "cold" definition for δR_c due to the higher B-gradient on the high-field-side. Consequently, non-local effects can contribute mainly at the lower frequency channels for the ECE interpretation.

According to Eq.(1), the spectral intensity $I_\omega = I_\omega(a)$ is calculated with given $n_e(r)$ and $T_e(r)$ profiles which are mapped to the horizontal ECE chord (straight line assumed) with $N_\parallel = 0$. The requested values of the absorption coefficient $\alpha_\omega(s')$ (and also $\eta_\omega(s')$) are evaluated corresponding to Ref. [3], $N_\perp$ is obtained within the tracing from the hot dielectric tensor. I_ω is averaged (integrated) with respect to the finite band width of all ECE frequency channels, getting $\langle I_\omega \rangle$. According to Eq.(2), an averaged T_{rad} profile is obtained from the simulated $\langle I_\omega \rangle$ spectrum, which can be compared with the measured ECE data; see Fig. 1. In addition, a definition of the position along the ECE chord corresponding to T_{rad} for each channel is needed. Here, some freedom exists. The most simple, but fairly inaccurate definition is used for the W7-AS ECE diagnostic, namely the "cold" resonance position for the central frequency of each channel, and the spatial uncertainty is only defined by the frequency width, δf. An improvement is obtained by using the position of the maximum of the integrand in Eq.(1) averaged over the width of the ECE channel. This position is always "inward-shifted", i.e. to higher B, compared to the "cold" resonance position. Since the balance of emission and reabsorption is fairy asymmet-

ric with respect to this maximum in s', an integral definition appears to be more appropriate: the position s_* is defined by $\langle I_\omega(s_*)\rangle = 0.5\,\langle I_\omega\rangle$ as "weighted center" of the emission line. This definition leads to an additional "inward-shift". Furthermore, the spatial extension of the emission zone for each channel is defined as the range with 90% contribution to the (central) I_ω. Then, the bounds s_{min} and s_{max}, are obtained from the conditions $\langle I_\omega(s_{min})\rangle = 0.05\,\langle I_\omega\rangle$ and $\langle I_\omega(s_{max})\rangle = 0.95\,\langle I_\omega\rangle$. Of course, this definition contents some freedom, but it gives the rule for a reasonable estimation of the spatial resolution. In fact, only the location of "cold" resonance is known *a priori*, and $s_{max} \lesssim R_c$. However, s_{min} contains the requested information about the spatial resolution.

A low density ($n_e \simeq 2\,10^{19}$ m^{-3}) ECRH discharge (1.2 MW heating with X2-mode at 140 GHz) with high temperature ($T_e \simeq 6$ keV) and very steep gradient (T_e' nearly 1 keV/cm) is a well suited scenario for the analysis. The highly focused ECRH with on-axis deposition results in a highly peaked T_e profile; see Ref. [4]. A suprathermal electron population is clearly indicated in the low frequency channels of the ECE diagnostic; see Fig. 1. After switching-off the ECRH, the suprathermal feature disappears on a much faster time-scale compared to the T_{rad} decay found in the "thermal" channels. The simulated T_{rad} spectrum is calculated with given n_e and T_e profiles (fits to Thomson scattering and ECE data).

The simulation is performed for all 24 ECE channels covering the range from 130 to 153 GHz (with a gap around the ECRH frequency at 140 GHz). For this simulation, a vacuum coordinate transform (for the density and temperature to the ECE chord) was used for simplicity. This approach is well sufficient to analyse the effects of the non-locality of the ECE emission, but not for the T_e-profile estimation. Here, the Shafranov shift as well as the diamagnetic effect must be included. For this type of discharges, however, equilibrium calculations with the pressure and the toroidal current density profile, both being highly peaked, are very expensive (poor radial resolution in the VMEC code close to the axis since an equidistant r^2-grid is used). Omitting the β-effects in the coordinate transform acts like outward-shift (to lower frequencies) of the T_{rad} spectrum. Furthermore, an additional uncertainty is indicated in the measured ECE spectra (a typically needed inward-shift of about 1 cm). With a sufficiently accurate transform, however, $T_e(r)$ profiles can be

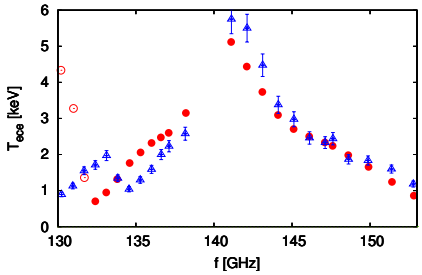

Figure 1: Calculated radiative temperature distribution over the used frequency channels. Bandwidth for each channel is equal 350 MHz.

mapped to all frequency channels of an ECE system within a fitting procedure. Then, the simulated and the measured I_ω are compared, and the problem of the non-locality of the emission is completely treated. All inaccuracies with the positioning of a "local" T_{rad} value for only one ECE channel diasappears. This approach is used within the integrated data analysis (IDA) concept for W7-X.

In the three lower channels, which correspond to the outer radii with low densities and temperatures, also a non-thermal feature appears in the simulated T_{rad} spectrum equivalent to the ECE feature. Strongly down-shifted emission (mainly from the central part) is only partly reabsorbed (small α_ω at these outer radii). As an illustration, profiles of the absorbtion coefficient $\alpha_\omega(R)$ (reabsorption omitted) are shown in Fig. 2a for three different channels. For two channels, the "cold" resonance is located nearly symmetrically in r (i.e. to nearly identical n_e and T_e), and the last one corresponds to an outer radius with the non-thermal feature. The shape of $\alpha_\omega(R)$ for the high-field-side channel is very narrow, but much broader for the corresponding low-field-side one. The decreased $\partial B/\partial R$ at the low-field-side cannot explain alone this effect, the strong gradients of T_e are mainly responsible for this difference. However, with the reabsorption included (exponential factor in the integrand in Eq.(1)) the "real" width of the emission line is sufficiently narrowed, but it exceeds the estimate for the spatial resolution at least for intermediate frequencies at the low-field-side. For the lowest frequency channel, the reabsorption is much too small to allow for a "local" T_{rad} evaluation.

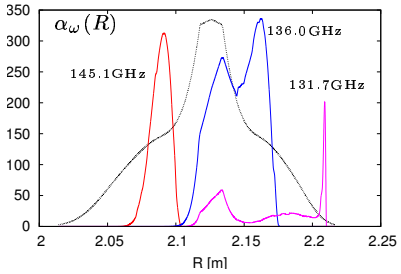

Figure 2a: Profiles of the absorption coefficient for different frequency channels. For comparison, the inferred $T_e(R)$ profile is also shown.

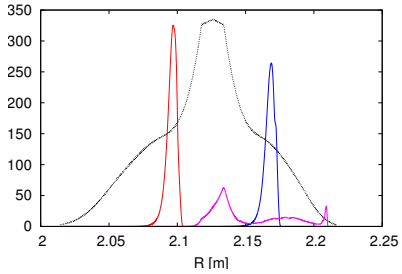

Figure 2b: Profiles of emission coefficient with reabsorption (integrand function for I_ω in Eq.(1)); equivalent to Fig.2a.

With mapping from frequency channels to the major radius coordinate R (which is with an offset equivalent to the chord coordinate s in Eq.(1)), $T_{rad}(R)$ is shown in Fig. 3. For the mapping, both the "cold" resonance position of the central frequency in each channel (triangles) and the "non-local" evaluation (circles, whith $R = R_*$ corresponding to the s_* definition) are used. As expected, the profile $T_{rad}(R_*)$ with the non-local emission

positioning has a noticable high-field-side shift with respect to the profile in local ("cold") approach. The radial bars given in Fig. 3, determinate for each channel the spatial resolution of ECE diagnostic (defined equivalent to s_{min} and s_{max}). The "cold" resonance definition of R almost coincides with the right-side bar, while the left-side bars determine the real width of the emission line. Please note, that the radial bars on the high-field-side are smaller than in low field side, especially on periphery. The size of the spatial resolution is noticably higher than the one obtained from the 1st order relativistic correction. For the low-field-side channels, a spatial resolution δR of about $2 \div 3$ cm is obtained in comparison to δR_r of about 1 cm.

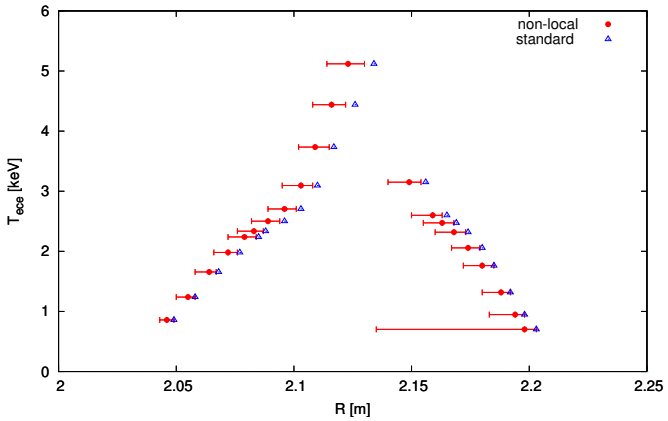

Figure 3: Calculated $T_{rad}(R)$ profiles. Circles show the profile interpreted as $T_{rad}(R_*)$, where R_* is the emission location; triangles show the same profile, but interpreted as standard one, $T_{rad}(R_c)$ with R_c taken as the "cold" resonance location.

The degradation of the spatial resolution of the ECE data evaluation becomes significant at high electron temperatures. With the non-local evaluation of the emission zone, the T_{rad} profiles have a systematic shift to the high-field-side compared to the usual "cold" resonance (local) positioning. Moreover, a strong T_e gradient leads to an additional asymmetry in the ECE profiles. For the W7-AS scenarios with a highly peaked T_e profile, only the high-field-side part of the ECE spectrum allows for an estimation of the "local" electron temperature.

1. V. Tribaldos, *Spatial Resolution of ECE for JET Typical Parameters*, Report EFDA-JET (2000)
2. G. Bekefi, *Radiation Processes in Plasmas* (John Willey & Sohns, New York, 1966)
3. M. Bornatici at al., *Nuclear Fusion* **23** 1153 (1983)
4. H. Maaßberg et al., *Phys. Plasmas* **7** 295 (2000)